Multiple-Ligand Binding in CYP2A6: Probing Mechanisms of Cytochrome P450 Cooperativity by Assessing Substrate Dynamics[†]

John P. Harrelson,*[,‡] William M. Atkins,[§] and Sidney D. Nelson[§]

School of Pharmacy, Pacific University, HPC-Ste 451, Hillsboro, Oregon 97123, and Department of Medicinal Chemistry, University of Washington, Box 357610, Seattle, Washington 98195

Received October 9, 2007; Revised Manuscript Received January 2, 2008

ABSTRACT: The contribution of ligand dynamics to CYP allosterism has not been considered in detail. On the basis of a previous study, we hypothesized that CYP2A6 and CYP2E1 accommodate multiple xylene ligands. As a result, the intramolecular $(k_H/k_D)_{obs}$ values observed for some xylene isomers are expected to be dependent on ligand concentration with contributions from [CYP·xylene] and [CYP·xylene·xylene], etc. To explore this possibility and the utility of kinetic isotope effects in characterizing allosteric CYP behavior, steady state kinetics, product ratios, and $(k_H/k_D)_{obs}$ values for CYP2E1 and CYP2A6 oxidation of *m*-xylene-α-$^2H_3$ and *p*-xylene-α-$^2H_3$ were determined. Evidence is presented that CYP2A6 accommodates multiple ligands and that intramolecular isotope effect experiments can provide insight into the mechanisms of multiple-ligand binding. CYP2A6 exhibited cooperative kinetics for *m*-xylene-α-$^2H_3$ oxidation and a concentration-dependent decrease in the *m*-methylbenzylalcohol:2,4-dimethylphenol product ratio (9.8 ± 0.1 and 4.8 ± 0.3 at 2.5 μM and 1 mM, respectively). Heterotropic effects were observed as well, as incubations containing both 15 μM *m*-xylene-α-$^2H_3$ and 200 μM *p*-xylene resulted in further reduction of the product ratio (2.4 ± 0.2). When *p*-xylene (60 μM) was replaced with deuterium-labeled d_6-*p*-xylene (60 μM), an intermolecular competitive inverse isotope effect on 2,4-dimethylphenol formation [$(k_H/k_D)_{obs} = 0.49$] was observed, indicating that *p*-xylene exerts heterotropic effects by residing in the active site simultaneously with *m*-xylene. The data indicate that there is a concentration-dependent decrease in the reorientation rate of *m*-xylene, as no increase in $(k_H/k_D)_{obs}$ was observed in the presence of an increased level of metabolic switching. That is, the accommodation of a second xylene molecule in the active site leads to a decrease in substrate dynamics.

Cytochromes P450 (CYP or P450)[1] are heme-containing enzymes that catalyze the oxidative metabolism of endogenous and exogenous compounds, to metabolites that are usually more water soluble. CYPs are involved in many important biological processes, including hormone synthesis and clearance of drugs and other chemicals, and in some cases, they also contribute to carcinogenic and toxic processes. Due to the important and varied roles that CYPs play, a substantial effort to characterize these enzymes continues, with the goal of predicting isoform selectivity of new drug candidates, rates of metabolite formation, product selectivity, and the formation of toxic products (*1*).

The mechanistic characterization of substrate−CYP interactions has been especially challenging since, in many instances, a single enzyme can bind a variety of substrates or multiple substrates simultaneously and generate multiple products from a single substrate. It is now well-known that the binding of multiple substrates or other types of effector molecules (e.g., cytochrome b_5 or metal ions) can alter binding affinities, product formation rates, and product selectivity and lead to non-Michaelis–Menten kinetics (i.e., allosterism or cooperativity) (*2–6*).

Generally, two mechanistic models have been proposed to explain multiple-ligand binding and the observation of atypical kinetics in P450 systems (*3, 7*). One model involves the binding of the effector molecule at a site that is some distance from the active site, which then induces a conformational change in the enzyme that alters the active site space. A second model involves a scenario in which multiple ligands can bind simultaneously within a fluid P450 active site. This second model implies that substrate orientation in the active site may involve not only ligand−protein interactions but also ligand−ligand interactions. There are data to support both models (*2, 4, 6, 8–17*). This research has been reviewed recently, and it appears that the applicable mechanism is dependent on a number of factors, including the identities of the CYP isoform, the substrate, and the effector molecule (*3, 7*).

Certainly, an important development in the characterization of substrate−CYP interactions has been the recent structural information about these interactions. A variety of tools have been used to investigate CYP structure, including X-ray

[†] This work was supported by NIH Grant GM 32165 and the UW NIEHS-sponsored Center for Ecogenetics and Environmental Health (NIEHS Grant P30ES07033).

* To whom correspondence should be addressed. E-mail: harrelsonj@pacificu.edu. Telephone: (503) 352-7292. Fax: (503) 352-7270.

[‡] Pacific University.

[§] University of Washington.

[1] Abbreviations: CYP or P450, cytochrome P450; k_H/k_D, intrinsic isotope effect; $(k_H/k_D)_{obs}$, measured isotope effect; MBA, *m*-methylbenzylalcohol; DMP, 2,4-dimethylphenol.

10.1021/bi702020y CCC: $40.75
Published on Web 02/05/2008

crystallography, mechanism-based inactivators, photoaffinity labeling, site-directed mutagenesis, and homology modeling. These techniques have been effective in the identification of residues that are important for function (*18, 19*), substrate selectivity (*20*), product selectivity (*21*), and cooperative kinetics (*22*). Interestingly, the static crystal structures of modified human CYPs have provided insight into the dynamic nature of the CYPs. In some structures, the substrate is positioned so far from the heme that some motion or translation by the substrate and/or protein is required for substrate oxidation (*23*). In other cases, the structural changes observed in comparisons of the substrate-free versus substrate-bound structures are indicative of significant protein motion (*24, 25*). However, details about protein and substrate dynamics remain unknown, and new methods are required to elucidate mechanisms of substrate binding and orientation, product selectivity, and multiple-ligand binding. Ultimately, this type of dynamic information should contribute to the development of more accurate models and improve in vitro to in vivo kinetic predictions.

Currently, there are several tools that can provide information about CYP and/or substrate dynamics. CO-flash photolysis has been effective at revealing information about the overall flexibility of P450 enzymes (*26*). Fluorescence studies have also been used to investigate protein dynamics (*27–29*). Solid state NMR was recently used to investigate amino acid motion upon substrate binding in $P450_{BM-3}$ (*30*). A solid state NMR method was also used to study P450cam and provided evidence that the substrate, adamantane, undergoes rapid motion within the P450cam active site (*31*).

Isotope effect experiments have also been used to characterize P450−substrate interactions. Specifically, they have been used to study the mechanisms that can lead to the formation of multiple products from a single substrate (i.e., metabolic switching) (*32*). For example, a combination of noncompetitive and competitive intermolecular isotope effect experiments was used to determine that the metabolism of testosterone by CYP2C11 occurs via a dissociative mechanism (*33*). Recently, similar experiments were used to demonstrate that CYP1A2-mediated metabolism of caffeine occurs via a nondissociative mechanism (*34*).

Indeed, deuterium isotope effect experiments have contributed considerably to our understanding of P450 enzymes (e.g., mechanisms of substrate oxidation, enzyme structure, substrate dynamics, and mechanisms of metabolic switching) (*35*). With appropriate experimental design, isotope effect experiments might also contribute to our understanding of substrate dynamics in relation to multiple-substrate binding. It has already been reported that isotope effect experiments can be used to determine the presence of two substrates in a single P450 active site (*15*).

Intramolecular isotope effect experiments that utilize symmetrical and selectively deuterium-labeled substrates have been used to study substrate dynamics (*35–39*). In the experiments reported here, a symmetrical substrate is labeled with deuterium atoms at one site of the molecule but is unlabeled at a symmetrically related site (Figure 1). In some circumstances, the value of the intramolecular $(k_H/k_D)_{obs}$ can indicate the relative rate of reorientation of these substrates.

CYP3A4 is one of the most studied enzymes with regard to P450 cooperativity. However, it is apparent that other drug-metabolizing CYPs and bacterial P450s are also able

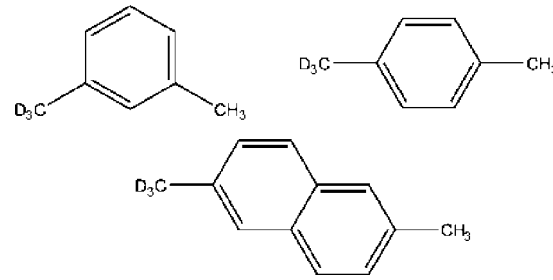

FIGURE 1: Examples of selectively deuterium-labeled substrates used in intramolecular isotope effect experiments.

to accommodate multiple ligands (*3, 14, 15, 40*). Previously, we observed that the intramolecular $(k_H/k_D)_{obs}$ values determined for CYP2E1- and CYP2A6-catalyzed oxidation of *p*-xylene-α-$^2H_3$ and 2-$^2H_3$,6-dimethylnaphthalene, although statistically significant, were not profoundly different (6.04 ± 0.26 and 5.50 ± 0.47 for CYP2E1 and 5.53 ± 0.19 and 4.96 ± 0.22 for CYP2A6, respectively) (*39*). Since the observed isotope effect is dependent on the rate of interchange of protio and deutero sites, these minor differences in $(k_H/k_D)_{obs}$ suggest that the interchange rates for these two substrates are similar even though these compounds span a rather large range of area and volume (27 and 51 Å^2 and 103 and 271 Å^3, respectively). This would mean that *p*-xylene and dimethylnaphthalene reorient at approximately the same rate, despite the difference in size (*36*). Theoretically, the enzyme active site structure should hinder dimethylnaphthalene dynamics to a greater extent in comparison to *p*-xylene. Considering the dynamic nature of CYPs, one explanation for similar reorientation rates for *p*-xylene and dimethylnaphthalene is that CYP2A6 and CYP2E1 may undergo conformational changes to accommodate larger substrates (e.g., dimethylnaphthalene) and provide, on average, a "roomier" active site that allows the rate of protio−deutero interchange to be maintained in going from *p*-xylene to dimethylnaphthalene. Another explanation is that the $(k_H/k_D)_{obs}$ values observed for xylene substrates are generated by the presence of two xylene molecules bound simultaneously to the CYP. Considering the high substrate concentrations used for the experiments (1 mM), this latter scenario seems plausible. On the basis of these data, we hypothesized that these two isoforms may accommodate multiple xylene ligands. Furthermore, if this hypothesis is true, then the intramolecular $(k_H/k_D)_{obs}$ values observed for some xylene isomers are generated from the presence of two ligands, even though it is widely believed that both isoforms have relatively small active sites compared to other CYPs. To test these two hypotheses, kinetic profiles and product branching ratios for CYP2A6- and CYP2E1-mediated oxidation of *m*-xylene-α-$^2H_3$ and *p*-xylene-α-$^2H_3$ were determined. Furthermore, we hypothesize that intramolecular isotope effects can serve as a tool for investigating the effect of multiple-ligand binding on substrate dynamics. To test this hypothesis, intramolecular deuterium isotope effects were determined for CYP2E1 and CYP2A6 using selectively labeled *m*- and *p*-xylenes at various concentrations. For substrate−P450 complexes that bind multiple substrates, we expected to see significant changes in $(k_H/k_D)_{obs}$ (most likely suppression) and/or a change in product ratios.

MATERIALS AND METHODS

Chemicals. The synthesis and characterization of *m*-xylene-α-$^2H_3$ and *p*-xylene-α-$^2H_3$ were described previously (*39*). Supersomes (human CYP2E1 and human CYP2A6 with P450 reductase and cytochrome b_5) and insect cell control microsomes were from BD Gentest. *p*-Xylene, *p*-xylene-α,α,α,α′,α′,α′-d_6, methyl 3-methylbenzoate, methyl 4-methylbenzoate, lithium aluminum deuteride (LAD), methanesulfonyl chloride, *N*,*N*-diisopropylethylamine (EDIPA), pentane, BSTFA, NADPH, *m*-methylbenzylalcohol, 2,4-dimethylphenol, and *p*-methylbenzylalcohol were purchased from Sigma-Aldrich. Methanol was purchased from Fisher. The DB-5 gas chromatography capillary column was from J&W Scientific (Folsom, CA). The Econosil C18 column was purchased from Alltech.

Kinetic Experiments, Determination of Intramolecular ($k_H/k_D)_{obs}$ Values, and Product Ratio Quantitation for the Hydroxylation of m-Xylene-α-$^2H_3$ and p-Xylene-α-$^2H_3$ by CYP2E1 and CYP2A6. Incubations contained 50−100 pmol CYP2E1 or CYP2A6 Supersomes in 50 mM potassium phosphate buffer (pH 7.4) in glass test tubes in a total volume of 500 μL. Substrate concentrations ranged from 1 μM to 5 mM (in methanol) depending on the substrate. The total methanol concentration was 1% for all samples (v/v). P450, buffer, and substrate were preincubated for 3 min at 37 °C, and then reactions were initiated by the addition of NADPH (final concentration of 1 mM). The incubation period was determined by linearity studies (product as a function of time). The incubations proceeded for 5.5−7.5 min depending on the isoform and substrate under study and then were terminated and extracted twice with 3 mL of ice-cold pentane. For quantification purposes, 100 pmol of either *m*-methylbenzylalcohol or *p*-methylbenzylalcohol was added as an internal standard before extraction. The pentane layers were combined and dried with magnesium sulfate. The magnesium sulfate was removed by centrifugation, and the pentane layers were evaporated to approximately 30 μL with dry N_2. Derivatization of the hydroxylated metabolites was achieved by the addition of 100 μL of a BSTFA/ethyl acetate mixture (1:1) and heating at 50 °C for 30 min. The derivatized samples were then analyzed by GC−MS. The interday coefficient of variation was <8% for 2,4-dimethylphenol detection (10 pmol/mL), <18% for *m*-methylbenzylalcohol detection (10 pmol/mL), and <17% for *p*-methylbenzylalcohol (10 pmol/mL). A table of peak areas for the standards and low-concentration experimental samples, a typical standard curve, and a table of product formation rates with corresponding product ratios are available as Supporting Information. The data points in Figures 5−8 and the values reported in Tables 2−5 represent the average of three independent experimental samples generated over a 3 day period and do not represent the replicate analysis of a single sample. Controls included incubations with a high substrate concentration without P450.

Kinetic Analysis. Kinetic parameters were determined using nonlinear regression (Graph-Pad Prism 4) and the Hill equation or Michaelis–Menten model. Curves for nonlinear Eadie−Hofstee plots were generated by nonlinear regression using a two-site model with competition (*41*). Hill coefficients (n) were determined from the slope of log $v/(V_{max} - v)$ versus log[substrate] plots using substrate concentrations near the S_{50} ($0.1S_{50}$ to $1.5S_{50}$; R^2 values were all >0.99 for these plots).

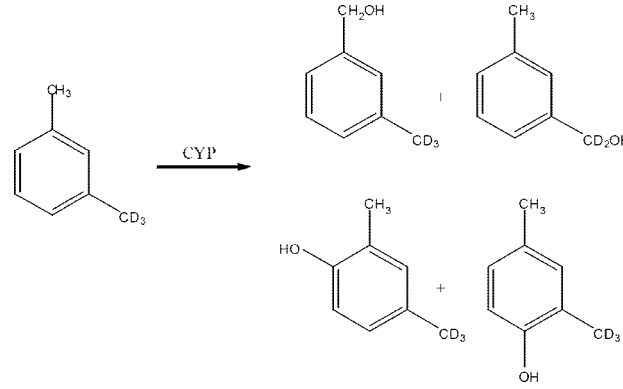

FIGURE 2: CYP-mediated formation of *m*-methylbenzylalcohol and 2,4-dimethylphenol from *m*-xylene-α-$^2H_3$ oxidation.

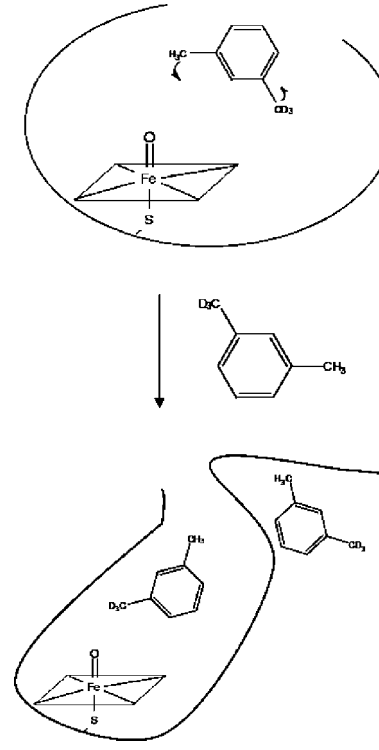

FIGURE 3: Simple conformational change model of two ligands binding to a P450.

Determination of Product Ratios and Intramolecular ($k_H/k_D)_{obs}$ Values for CYP2A6-Mediated Oxidation of m-Xylene-α-$^2H_3$ in the Presence of Unlabeled (d_0) and Labeled (d_6) p-Xylene (heterotropic experiments). Incubation conditions were similar to those described above except that the *m*-xylene-α-$^2H_3$ concentration was 15 μM (below the S_{50}). *p*-Xylene concentrations were either 60 μM (approximate K_M) or 200 μM (>3 times the approximate K_M). The experiment was conducted in triplicate. The product ratios and isotope effect values reported in Table 6 represent the average of three individual experimental samples. To measure changes in the product ratio (i.e., *m*-methylbenzylalcohol:2,4-dimethylphenol) for *m*-xylene-α-$^2H_3$ oxidation in the presence of *p*-xylene, the peak areas of the two metabolites were compared. The sensitivity of the GC−MS assay was greater for 2,4-dimethylphenol so the ratio of peak areas did not directly reflect the mole ratios for the two metabolites. To determine the mole ratios for the two products, the

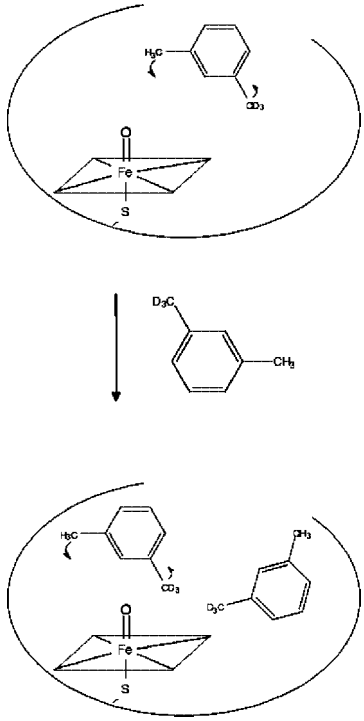

FIGURE 4: Simple model of two *m*-xylene molecules bound in a CYP active site simultaneously.

difference in sensitivity for the two metabolites was determined. For each metabolite, the peak area ratio compared to the *p*-methylbenzylalcohol internal standard was determined over a range of concentrations (picomoles of metabolite to picomoles of internal standard, 0.05, 0.1, 0.5, 1, and 3). Using these peak area ratios, it was determined that, on average, the assay was 1.44 (±0.08) times more sensitive for 2,4-dimethylphenol detection than for *m*-methylbenzylalcohol detection; this average value was determined from five standard curves. A table displaying the peak areas utilized to determine the product ratios under the various experimental conditions is available as Supporting Information.

GC−MS Analysis. Derivatized metabolites were analyzed with a Finnigan Trio 1000 mass spectrometer interfaced with a Hewlett-Packard 5890 gas chromatograph equipped with a DB-5 capillary column (30 m). The column head pressure was set to 5 psi with helium used as the carrier gas. The mass spectrometer was operated in the electron impact mode (EI) at −70 eV electron energy with source and interface temperatures set at 200 and 250 °C, respectively. Ions were detected in the selected ion monitoring mode (SIM). Xylene metabolites were injected on the column at an oven temperature of 40 °C, held at a constant temperature for 1 min, and eluted with a linear gradient of 3 °C/min to 180 °C. Monitored ions corresponded to the $[M - 15]^+$ fragments generated from the trimethylsilylated hydroxyl metabolites. Confirmation of the metabolite retention times was accomplished by comparison to the retention times of commercially available standards. Typical chromatograms for the metabolites were similar to those from previous studies; isotope effect values were calculated using the peak areas of ions with *m*/*z* 180, 181, 182, and 183 to correct for natural isotopic abundance and incomplete deuterium incorporation as previously described (*39*).

RESULTS

Experimental Rationale. The theory that explains how the rate of reorientation of selectively deuterium-labeled substrate molecules impacts the measured isotope effect [i.e., the observed isotope effect, $(k_H/k_D)_{obs}$] for substrate oxidation has been developed and is described by Scheme 1 and eq 1 (*35, 42*). The $(k_H/k_D)_{obs}$ for the oxidation of these types of substrates reflects the rate of reorientation (k_{43}) of the labeled and unlabeled sites on the substrate because as the rate of reorientation is slowed, the $(k_H/k_D)_{obs}$ decreases. That is, suppression of the intrinsic isotope effect is observed when the rate of interchange between labeled and unlabeled regions of a molecule is slow compared to the rate of product formation (in eq 1, the intrinsic isotope effect for the oxidizing step is k_{45H}/k_{45D}, where k_{45H} is the rate constant associated with oxidation at the protium-containing methyl group and k_{45D} is the rate constant associated with oxidation at the deuterium-labeled methyl group).

$$(k_H/k_D)_{obs} = \frac{k_{45H}/k_{45D} + k_{45H}/k_{43}}{1 + k_{45H}/k_{43}} \quad (1)$$

This equation explains how the measured isotope effect, $(k_H/k_D)_{obs}$, changes as a function of the reorientation rate (k_{43}). As k_{43} increases, the k_{45H}/k_{43} term approaches zero and the intrinisic isotope effect (k_{45H}/k_{45D}) will be expressed. Full expression of the intrinsic isotope effect [i.e., maximal values of $(k_H/k_D)_{obs}$] is expected for compounds that can reorient rapidly (i.e., short distances between labeled and unlabeled methyl groups). Recently, this technique was used to elucidate the influence of phenylalanine 87 on substrate dynamics in $P450_{BM-3}$ (*38*).

However, if there is an alternate site on the substrate that is also available for oxidation then suppressed isotope effects may not be observed and $(k_H/k_D)_{obs}$ will approach the intrinsic isotope effect. This is known as metabolic switching (or isotopically sensitive branching) and is a form of branching (*42–44*).

Branching is a phenomenon in which there are alternative pathways that are not directly isotopically sensitive but that are in competition with the isotopically sensitive step. For example, the aromatic hydroxylation of *m*-xylene-α-$^2H_3$ (Figure 2) is an example of metabolic switching from benzylic oxidation (which involves the competition between ^1H atom abstraction at one methyl group vs ^2H atom abstraction at the other methyl group) to ring hydroxylation. A kinetic model has also been developed to determine the impact that branched pathways have on the value of $(k_H/k_D)_{obs}$ (*35, 43, 44*) (Scheme 2 and eq 2).

$$(k_H/k_D)_{obs} = \frac{k_{45H}/k_{45D} + k_{45H}/(k_{43} + k_{46})}{1 + k_{45H}/(k_{43} + k_{46})} \quad (2)$$

This equation explains how the measured isotope effect, $(k_H/k_D)_{obs}$, changes as a function of the reorientation rate (k_{43}) and the rate of metabolism at a "switch-to" site that is not isotopically labeled (k_{46}). As k_{43} and/or k_{46} increases, the "$k_{45H}/k_{43} + k_{46}$" term approaches zero and the intrinisic isotope effect (k_{45H}/k_{45D}) will be expressed.

When one considers CYPs' broad substrate selectivity, flexibility, and accommodation of multiple ligands, it is likely that some intramolecular isotope effect values are a reflection of the dynamics of two substrates binding to the enzyme. If

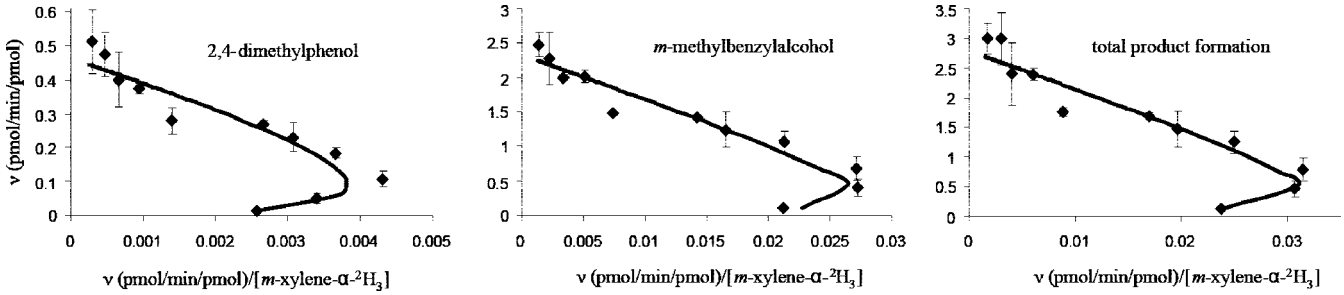

FIGURE 5: Eadie−Hofstee plots for 2,4-dimethylphenol, *m*-methylbenzylalcohol, and total product formation from CYP2A6-mediated *m*-xylene-α-$^2H_3$ oxidation. Concentration is expressed in micromolar. Each data point represents the average of three independent experimental samples. The error bars represent the associated standard deviations for these measurements.

Table 1: Effects of Substrate Dynamics (k_{43}) and Branching Rate (k_{46}) on $(k_H/k_D)_{obs}$ and Product Ratios

scenario	$(k_H/k_D)_{obs}$	product ratio
(1) ↓ k_{43}; no change in k_{46}	decreases	no change
(2) ↓ k_{43}; ↑ k_{46}	variable; depends on the ratio of $\Delta k_{43}/\Delta k_{46}$	increase in the branched product
(3) no change in k_{43}; ↑ k_{46}	increases	increase in the branched product
(4) ↑ k_{43}; ↑ k_{46}	increases	increase in the branched product

Table 2: Kinetic Pameters for CYP2A6-Catalyzed Oxidation of *m*-Xylene-α-$^2H_3$[a]

	V_{max} (pmol min^{-1} pmol^{-1})	S_{50} (μM)	V_{max}/S_{50}
total product	2.9 ± 0.3	74 ± 9	0.040
m-methylbenzylalcohol	2.4 ± 0.3	74 ± 14	0.032
2,4-dimethylphenol	0.50 ± 0.07	110 ± 19	0.005

[a] Values represent the average of three independent experimental samples.

Table 3: Kinetic Parameters for CYP2A6- and CYP2E1-Catalyzed Oxidation of *p*-Xylene-α-$^2H_3$[a]

	V_{max} (pmol min^{-1} pmol^{-1})	K_M (μM)	V_{max}/K_M
CYP2A6	1.3 ± 0.1	64 ± 9	0.019
CYP2E1	1.3 ± 0.1	72 ± 10	0.018

[a] Values represent the average of three independent experimental samples.

this is the case, then the observed intramolecular isotope effect will be a function of substrate concentration, since an additional substrate may introduce additional steric interactions that affect substrate reorientation.

On the basis of these considerations, intramolecular isotope effects provide a method of exploring multiple-ligand binding and, more significantly, the impact of multiple-ligand binding on substrate dynamics. Two scenarios can be imagined on the basis of the models of P450 allosterism described (vide supra). Using a simple conformational change model, a lone substrate in the active site undergoes rapid reorientation (Figure 3). The binding of a second ligand external to the active site leads to a change in the active site structure that on average is more restrictive and reduces the mobility of the other substrate within the active site.

The second model involves two ligands bound simultaneously in the active site. The first substrate binds and is dynamic (i.e., the substrate rapidly samples different orientations relative to the heme). Binding of a second ligand to the active site reduces the active site space available for substrate mobility and reorientation of isotopically distinct methyl groups (for both ligands) (Figure 4).

Both models predict a concentration-dependent suppression of the isotope effect if the available active site space is reduced (either by conformational changes or by the presence of another substrate in the active site) to a degree that substrate reorientation (k_{43}) is reduced. However, suppression of k_H/k_D is dependent not only on substrate orientation but also on the nature of multiple-ligand binding. If both substrates compete simultaneously for the active oxygenating species (Figure 4), then the enzyme again "has a choice" when presented with the labeled portion of one substrate and an unlabeled region from the second substrate. Therefore, the active oxygenating species may oxidize the more energetically favorable, unlabeled position of the other, competing substrate. In other words, these cases provide a mechanism for metabolic switching and an unmasking of the intrinsic isotope effect. Alternatively, only one substrate may have immediate access to the active oxygenating species (on the time scale of substrate oxidation). The crystal structure of two 9-aminophenanthrene molecules bound to P450eryF is an excellent static example of this type of "stacked" binding (*14*). In this case, an increase in the level of metabolic switching or a decrease in $(k_H/k_D)_{obs}$ can still be observed if the second substrate prevents rapid reorientation of the substrate that is positioned closer to the heme.

Since the observed intramolecular isotope effect, $(k_H/k_D)_{obs}$, is dependent on the rate of substrate reorientation (k_{43}) and the rate of metabolic switching (k_{46}) (eq 2), there are a number of concentration-dependent effects that could be observed when a CYP binds multiple ligands (Table 1). (1) A decrease in the substrate reorientation rate (k_{43}) due to steric crowding and no change in the branching rate (k_{46}); this would lead to suppression of the intramolecular $(k_H/k_D)_{obs}$ with an increase in substrate concentration. (2) A scenario in which there is a concentration-dependent decrease in the reorientation rate (k_{43}) and an increase in the level of metabolic switching (k_{46}) where the net effect on $(k_H/k_D)_{obs}$ would be dependent on the degree of change for each rate constant. In this scenario, the intramolecular $(k_H/k_D)_{obs}$ might not change even though there is a decrease in the reorientation rate (k_{43}): when the decrease in the reorientation rate (k_{43}) is matched by an equivalent increase in the branching rate (k_{46}), which can be observed as a change in product ratios. (3) There is no change in k_{43}, but there is an increase in the branching rate (k_{46}), leading to an increase in $(k_H/k_D)_{obs}$. (4) A scenario in which the accommodation of a second substrate allows for faster substrate reorientation rates (increase in k_{43}) and a simultaneous increase in the branching

Table 4: Product Ratios, Intramolecular $(k_H/k_D)_{obs}$ Values, and Reaction Velocities for CYP2E1-Mediated Oxidation of *p*-Xylene-α-$^2H_3$ and *m*-Xylene-α-$^2H_3$ at High and Low Substrate Concentrations[a]

	25 μM *p*-xylene-α-$^2H_3$	5 mM *p*-xylene-α-$^2H_3$	7.5 μM *m*-xylene-α-$^2H_3$	1 mM *m*-xylene-α-$^2H_3$
product ratio[b]	NA[c]	NA[c]	16.2 ± 1.3	19.3 ± 3.9
$(k_H/k_D)_{obs}$	5.20 ± 0.19	5.03 ± 0.43	5.85 ± 0.38	5.75 ± 0.12
v (pmol min^{-1} pmol^{-1})	0.24 ± 0.01	1.4 ± 0.05	0.10 ± 0.01	0.60 ± 0.07

[a] Values represent the average of three independent experimental samples. [b] No product ratio is shown for *p*-xylene because *p*-methylbenzylalcohol was the only product observed with this substrate. The product ratio is *m*-methylbenzylalcohol to 2,4-dimethylphenol. [c] Not available.

Table 5: Product Ratios, Intramolecular $(k_H/k_D)_{obs}$ Values, and Reaction Velocities for CYP2A6-Mediated Oxidation of *p*-Xylene-α-$^2H_3$ and *m*-Xylene-α-$^2H_3$ at High and Low Substrate Concentrations[a]

	25 μM *p*-xylene-α-$^2H_3$	5 mM *p*-xylene-α-$^2H_3$	2.5 μM *m*-xylene-α-$^2H_3$	1 mM *m*-xylene-α-$^2H_3$
product ratio[b]	NA[c]	NA[c]	9.8 ± 0.1	4.8 ± 0.3
$(k_H/k_D)_{obs}$	6.30 ± 0.41	5.07 ± 0.49	6.7 ± 0.4	6.6 ± 0.1
v (pmol min^{-1} pmol^{-1})	0.36 ± 0.02	1.2 ± 0.1	0.10 ± 0.02	3.0 ± 0.07

[a] Values represent the average of three independent experimental samples. [b] No product ratio is shown for *p*-xylene because *p*-methylbenzylalcohol was the only product observed with this substrate. Product ratio is *m*-methylbenzylalcohol to 2,4-dimethylphenol. [c] Not available.

Scheme 1: Rate Constants Involved when a P450 Enzyme (E) Catalyzes the Oxidation of a Substrate (S) that Can Be Metabolized at a Deuterium-Containing Carbon (EOS_D) or a Protium-Containing Carbon (EOS_H)[a]

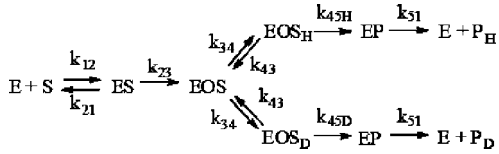

[a] EOS represents substrate bound to the P450 that has formed the active oxidizing species. P_H and P_D represent products from oxidation at the protium-containing site and deuterium-containing site, respectively. Thus, P_H contains all the deuterium atoms, and P_D has lost one deuterium.

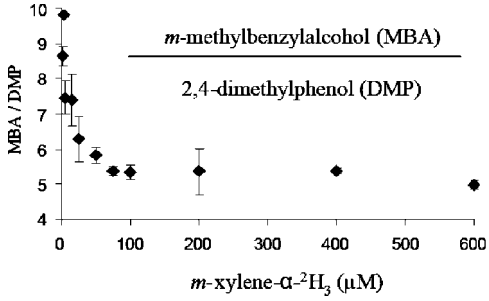

FIGURE 6: *m*-Methylbenzylalcohol:2,4-dimethylphenol product ratios for the CYP2A6-mediated oxidation of *m*-xylene-α-$^2H_3$ as a function of substrate concentration. Each data point represents the average of three independent experimental samples. The error bars represent the associated standard deviations for these measurements.

rate (k_{46}). Both of these effects would lead to an increase in $(k_H/k_D)_{obs}$. This scenario might apply when the accommodation of a second substrate results in an active site that is more spacious.

Kinetics of CYP2A6-Mediated Oxidation of m-Xylene-α-$^2H_3$. CYP2A6 oxidized *m*-xylene-α-$^2H_3$ to two products, *m*-methylbenzylalcohol and 2,4-dimethylphenol (Figure 2). At 5 μM substrate, formation of both products was linear for at least six minutes. All three (2,4-dimethylphenol, *m*-methylbenzylalcohol, and total product) Eadie−Hofstee plots deviated from linearity at low substrate concentrations, and the deviation was most apparent for 2,4-dimethylphenol formation (Figure 5). A higher degree of cooperativity for phenol formation was also revealed by the larger Hill

Scheme 2: Additional Rate Constants Involved when Oxidation Can Also Occur at an Alternative Site on the Substrate that Is Not Isotopically Sensitive but that Is in Competition with the Isotopically Sensitive Step (i.e., metabolic switching)[a]

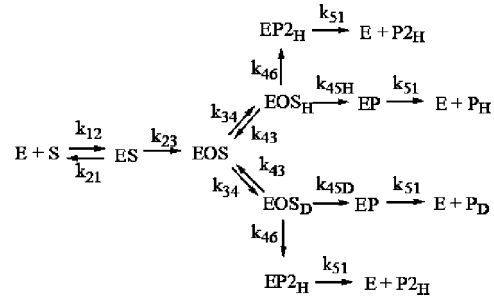

[a] $P2_H$ is the product formed from oxidation at the alternate site, such as ring hydroxylation for xylene.

coefficient ($n = 1.4$) for this product compared to that for benzylalcohol formation ($n = 1.1$).

For CYP2A6, *m*-methylbenzylalcohol is the major product at all concentrations but becomes less favored with an increase in substrate concentration. That is, the *m*-methylbenzylalcohol:2,4-dimethylphenol product ratio decreases from 9.8 ± 0.1 at 2.5 μM to 4.9 ± 0.7 at 1.75 mM (Figure 6). A complete table of product formation rates and the corresponding product ratios is available as Supporting Information.

The data were fit to the Hill equation to approximate kinetic parameters. The kinetic parameters for each product are summarized in Table 2. The V_{max} for benzylalcohol formation was nearly 5-fold higher than the V_{max} for phenol formation (2.4 ± 0.3 and 0.50 ± 0.07 pmol min^{-1} pmol^{-1}, respectively; $p < 0.004$). Small differences in S_{50} were also observed (74 ± 14 and 110 ± 19 μM for benzylalcohol and phenol formation, respectively; $p < 0.05$).

Kinetics of CYP2E1-Mediated Oxidation of m-Xylene-α-$^2H_3$. Like CYP2A6, CYP2E1 also catalyzes the oxidation of *m*-xylene-α-$^2H_3$ to two products, but *m*-methylbenzylalcohol is even more preferred (for *m*-methylbenzylalcohol, $V_{max} = 0.57 \pm 0.05$ pmol min^{-1} pmol^{-1} and $S_{50} = 54 \pm 4$ μM; for 2,4-dimethylphenol, $V_{max} = 0.026 \pm 0.001$ pmol min^{-1} pmol^{-1} and $K_M = 19 \pm 1.9$ μM). As a function of time, formation of both products was linear for at least 7.5

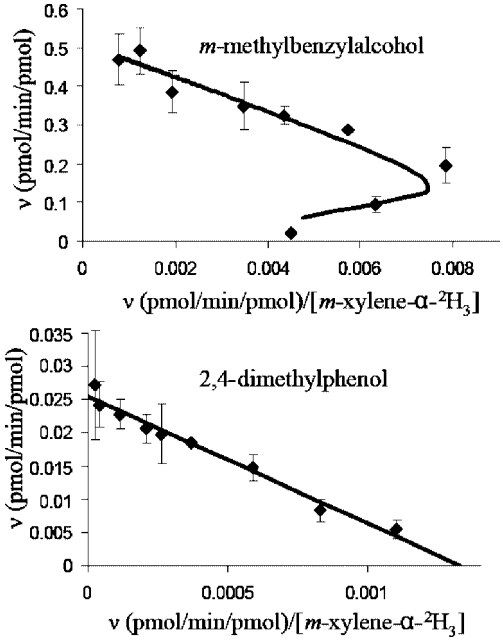

FIGURE 7: Eadie−Hofstee plots for *m*-methylbenzylalcohol and 2,4-dimethylphenol formation from CYP2E1-mediated *m*-xylene-α-$^2H_3$ oxidation. Concentration is expressed in micromolar. Each data point represents the average of three independent experimental samples. The error bars represent the associated standard deviations for these measurements.

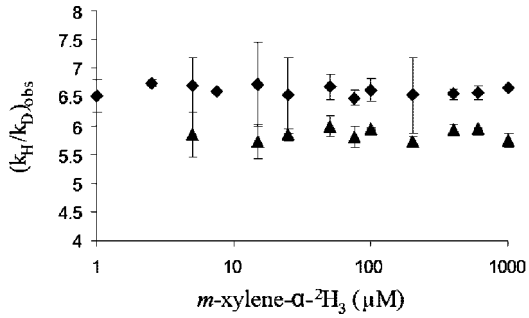

FIGURE 8: $(k_H/k_D)_{obs}$ values for the CYP2A6- and CYP2E1-mediated oxidation of *m*-xylene-α-$^2H_3$ as a function of substrate concentration: (◆) CYP2A6-mediated oxidation and (▲) CYP2E1-mediated oxidation. Each data point represents the average of three independent experimental samples. The error bars represent the associated standard deviations for these measurements.

min. Interestingly, an Eadie−Hofstee plot of *m*-methylbenzylalcohol formation deviated from linearity at low substrate concentrations while similar plots of the minor product were linear (Figure 7). Unlike the case for CYP2A6, a concentration-dependent change in product ratio was not observed (e.g., *m*-methylbenzylalcohol:2,4-dimethylphenol ratio = 16.2 ± 1.3 and 19.3 ± 3.9 at 7.5 μM and 1 mM, respectively).

Kinetics of CYP2A6- and CYP2E1-Mediated Oxidation of p-Xylene-α-$^2H_3$. For both isoforms, product formation was linear for at least 7.5 min and only one product was observed (*p*-methylbenzylalcohol). The kinetic parameters are summarized in Table 3; CYP2E1 and CYP2A6 displayed similar catalytic efficiencies for this substrate. Michaelis–Menten and Eadie−Hofstee plots showed that the kinetics for both enzymes were typical (i.e., hyperbolic Michaelis–Menten plots and linear Eadie−Hofstee plots). K_M values determined for CYP2A6 were used to determine appropriate concentrations for the heterotropic experiments described below.

Table 6: Product Ratios and $(k_H/k_D)_{obs}$ Values for CYP2A6-Mediated Oxidation of *m*-Xylene-α-$^2H_3$ and Effects of Unlabeled and Deuterium-Labeled *p*-Xylene[a]

substrate(s)	product ratio[b]	$(k_H/k_D)_{obs}$
m-xylene-α-$^2H_3$ (15 μM)	7.2 ± 0.6	6.98 ± 0.16
m-xylene-α-$^2H_3$ (1000 μM)	4.8 ± 0.3	6.62 ± 0.04
m-xylene-α-$^2H_3$ (15 μM) with *p*-xylene (60 μM)	6.8 ± 0.4	6.83 ± 0.06
m-xylene-α-$^2H_3$ (15 μM) with *p*-xylene (200 μM)	2.4 ± 0.2[c]	7.22 ± 0.48
m-xylene-α-$^2H_3$ (15 μM) with *p*-xylene-d_6 (60 μM)	3.3 ± 0.5[c]	6.65 ± 0.36
m-xylene-α-$^2H_3$ (15 μM) with *p*-xylene-d_6 (200 μM)	2.9 ± 0.5[c]	5.77 ± 0.45[d]

[a] Each value is the average of three incubations. [b] Product ratio is *m*-methylbenzylalcohol to 2,4-dimethylphenol. [c] $p < 0.002$ compared to *m*-xylene-α-$^2H_3$ (15 μM). [d] $p < 0.04$ compared to *m*-xylene-α-$^2H_3$ (15 μM) with *p*-xylene-d_6 (60 μM). $p < 0.025$ compared to *m*-xylene-α-$^2H_3$ (15 μM) with *p*-xylene (200 μM). $p < 0.01$ compared to *m*-xylene-α-$^2H_3$ (15 μM) with *p*-xylene (60 μM).

Determination of Intramolecular $(k_H/k_D)_{obs}$ Values as a Function of Substrate Concentration for CYP2A6- and CYP2E1-Mediated Oxidation of m-Xylene-α-$^2H_3$ and p-Xylene-α-$^2H_3$. Intramolecular $(k_H/k_D)_{obs}$ values were measured as a function of substrate concentration. No substrate concentration-dependent change in intramolecular $(k_H/k_D)_{obs}$ values was observed with either CYP2A6- or CYP2E1-catalyzed *m*-xylene-α-$^2H_3$ oxidation (Figure 8). The intramolecular $(k_H/k_D)_{obs}$ for CYP2E1-mediated oxidation of *p*-xylene-α-$^2H_3$ also did not change significantly as a function of concentration. As displayed in Table 4, at a *p*-xylene concentration of 25 μM, $(k_H/k_D)_{obs} = 5.20 \pm 0.19$, and at 5 mM *p*-xylene, $(k_H/k_D)_{obs} = 5.03 \pm 0.43$ ($p < 0.55$). CYP2A6-catalyzed *p*-xylene oxidation displayed an isotope effect suppression that was concentration-dependent and statistically significant but not dramatic (e.g., 6.30 ± 0.41 at 25 μM and 5.07 ± 0.49 at 5 mM; $p < 0.03$) (Table 5).

Effects of Unlabeled (d_0) and Labeled (d_6) p-Xylene on the Product Ratios and Intramolecular $(k_H/k_D)_{obs}$ for CYP2A6-Mediated Oxidation of m-Xylene-α-$^2H_3$ (heterotropic experiments). Since CYP2A6 exhibited nonlinear Eadie−Hofstee plots for *m*-xylene-α-$^2H_3$ oxidation and also a change in product ratio (*m*-methylbenzylalcohol:2,4-dimethylphenol) that was concentration-dependent, this isoform−substrate pair was tested further for multiple-ligand binding effects. Incubations with deuterium-labeled *p*-xylene (d_6; both methyl groups labeled) at 60 μM (approximate K_M for *p*-xylene) resulted in a dramatic change in the ratio of products obtained from *m*-xylene; the effect was more dramatic than the change observed with the highest concentration of *m*-xylene-α-$^2H_3$ (product ratio of 7.2 at 15 μM *m*-xylene, product ratio of 4.8 at 1 mM *m*-xylene, product ratio of 3.3 at 15 μM *m*-xylene and 60 μM d_6-*p*-xylene) (Table 6). No dramatic change was observed with 60 μM unlabeled *p*-xylene (product ratio of 6.8). However, a significant change in branching ratio was observed with 60 μM d_6-labeled *p*-xylene (product ratio of 3.3) and with higher concentrations of unlabeled *p*-xylene (200 μM; product ratio of 2.4). Intramolecular $(k_H/k_D)_{obs}$ values for *m*-xylene-α-$^2H_3$ oxidation were statistically the same under all conditions except for incubations containing 200 μM d_6-*p*-xylene; $(k_H/k_D)_{obs}$ values observed under these conditions were statistically different

from those observed under all other conditions, including those that contained only *m*-xylene-α-$^2H_3$ (this was true at all concentrations of *m*-xylene-α-$^2H_3$, from 1 μM to 1.75 mM) (Figure 8 and Table 6).

DISCUSSION

The work presented here addresses two questions. (1) Can intramolecular isotope effects be used to provide insight into the molecular mechanisms of P450 allosterism? That is, do intramolecular $(k_H/k_D)_{obs}$ values, in some cases, reflect the dynamics of multiple substrates bound to the enzyme? (2) Do CYP2E1 and CYP2A6 accommodate multiple substrates? This latter question will be addressed first.

There are a number of methods and indicators based on the steady state velocity of product formation for observing P450 allosterism and/or multiple-ligand binding. For example, nonlinear Eadie−Hofstee plots, product-dependent S_{50} or K_M values for a single substrate, and product ratios that are dependent on substrate concentration all have been widely documented. However, these methods provide no information about rates of substrate reorientation. Furthermore, equilibrium binding in the absence of catalytic turnover has also been used to demonstrate multiple ligands bind to several CYPs (*45*).

With regard to drug-metabolizing P450s, allosterism and multiple-ligand binding have been most commonly reported for CYP3A4 and CYP2C9, although they have also been observed with many other isoforms (*13, 40, 46*). It is widely accepted, on the basis of substrate selectivity, that the active sites for CYP2E1 and CYP2A6 are relatively small, in comparison. This has led to the assumption that these isoforms are unlikely to exhibit atypical kinetics via multiple-ligand binding, especially if the mechanism of CYP allosterism involves multiple ligands bound simultaneously to the active site. However, considering P450 promiscuity and the crystallographic evidence that substrate binding may involve varying degrees of conformational change [including CYP2A6 (*47*)], it seems reasonable that CYP2E1 and CYP2A6 may also accommodate multiple substrates. There is one direct report of cooperative kinetics for CYP2E1; they were observed for CYP2E1-mediated 7-ethoxycoumarin deethylation (Hill constant of 1.6) (*20*). However, a full kinetic analysis (e.g., Eadie−Hofstee plot) was not provided. In another report, the authors displayed Eadie−Hofstee plots for CYP2A6- and CYP2E1-mediated phenacetin O-deethylation that appear to deviate from linearity at low substrate concentrations. However, no comment was made regarding the cooperative behavior (*48*). In general, examples of multiple-ligand binding in CYP2A6 and CYP2E1 are not as well documented as for other CYPs.

The current study indicates that CYP2A6 simultaneously accommodates multiple ligands. CYP2A6 catalyzes the oxidation of *m*-xylene-α-$^2H_3$ to two products (Figure 2) (note that aromatic hydroxylation at the 4- and 6-positions was analyzed as the same product). Eadie−Hofstee plots (v vs v/[S]) of total product, *m*-methylbenzylalcohol, and 2,4-dimethylphenol formation for the CYP2A6-catalyzed oxidation of *m*-xylene-α-$^2H_3$ all deviated from linearity at low substrate concentrations. Nonlinearity due to increased rates of enzyme degradation at low substrate concentrations was ruled out; product formation was linear at low substrate concentrations, within the incubation period selected for the kinetic study. This cooperative effect was most significant for 2,4-dimethylphenol ($n = 1.4$) (Figure 5).

Stronger evidence that CYP2A6 accommodates two *m*-xylene molecules comes from the significant change in product ratios that is observed with an increase in substrate concentration (e.g., *m*-methylbenzylalcohol:2,4-dimethylphenol ratios of 9.8 ± 0.1 and 4.8 ± 0.3 at 2.5 μM and 1 mM *m*-xylene-α-$^2H_3$, respectively) (Figure 6 and Table 5). Compared to aromatic hydroxylation, benzylic positions are generally more reactive and more susceptible to hydroxylation; one explanation for this observation is that benzylic hydroxylation allows for resonance stabilization of the transition state, while aromatic hydroxylation leads to a transition state that involves a loss of aromaticity. The change in product ratio supports a model in which binding of the second substrate leads to active site crowding, whereby reorientation of the molecule is slowed and the active oxygenating species is presented with the unlabeled methyl group less often (on the time scale of the oxidizing step). In this model, at low substrate concentrations, there are three possible sites for oxidation that reorient rapidly: the unlabeled methyl group, the deuterium-labeled methyl group, and the aromatic ring. At higher concentrations, there are still three possible sites of oxidation, but steric constraints prevent their rapid interchange. The enzyme is "forced" to oxidize a less favorable site (i.e., on either the aromatic ring or the deuterium-labeled methyl group). To summarize, in this model, aromatic hydroxylation is increased at higher concentrations because the substrates are not as dynamic due to steric crowding of the active site (either due to multiple substrates in the active site or because of a conformational change). The site of reaction is determined more by steric binding constraints and less by chemical reactivity.

If substrates are less dynamic (i.e., the reorientation rate is decreased), then should not this be reflected in a suppression of the measured intramolecular isotope effect $[(k_H/k_D)_{obs}]$? On the basis of a model that takes into account only reactions at the labeled and unlabeled methyl groups (i.e., benzylic hydroxylation), this is the case (eq 1 and Scheme 1). As the reorientation rate (k_{43}) is reduced, the term k_{45H}/k_{43} becomes larger, resulting in suppression of the observed intramolecular isotope effect $[(k_H/k_D)_{obs}]$. However, when a model is used that also accounts for the effect of metabolic switching (k_{46}) on $(k_H/k_D)_{obs}$, it is evident that reduced substrate dynamics (decreased k_{43}) may not necessarily lead to suppression of the measured intramolecular isotope effect, if the branching rate (k_{46}) is increasing simultaneously (*44*). That is, two different effects can result from the reduced dynamics of deuterium-labeled substrates: (1) a change in the measured intramolecular isotope effect or (2) a change in the extent of isotopically sensitive metabolic switching.

As described in the experimental rationale section (Table 1), there are several scenarios that are possible in an intramolecular isotope effect experiment that involves metabolic switching. In the case of CYP2A6, a concentration-dependent increase in switching to the product resulting from aromatic hydroxylation (2,4-dimethylphenol) was observed while the observed intramolecular isotope effect [i.e., $(k_H/k_D)_{obs}$] did not change (Figures 6 and 8 and Table 6). These results rule out scenarios 1, 3, and 4 and suggest that for CYP2A6−*m*-xylene complexes, the concentration-dependent

increase in metabolic switching is countered by a similar decline in substrate reorientation (increased metabolic switching without a decrease in reorientation would lead to an increase in the observed isotope effect). To summarize, the data suggest that accommodation of a second substrate leads to a decrease in substrate dynamics to the degree that the less energetically favored product is formed due to steric crowding.

Another explanation for the observation that the isotope effect does not increase with increased branching is that the intrinsic isotope effect is already fully expressed. The intrinsic isotope effect was previously estimated for *o*-xylene. The intramolecular isotope effect [$(k_H/k_D)_{obs}$] determined for CYP2A6-catalyzed *o*-xylene-α-$^2H_3$ oxidation was 11.46 ± 0.28, and branching was not observed with this substrate (*39*). Therefore, interchange between labeled and unlabeled sites in this molecule is rapid and should provide a reasonable approximation of the general intrinsic isotope effect for benzylic hydroxylation of xylenes in CYP2A6. Obviously, the observed isotope effect of 5.8 is significantly below the intrinisic limit, and therefore, it is unlikely that it represents a fully expressed intrinsic isotope effect.

Although the evidence presented thus far suggests CYP2A6 accommodates multiple *m*-xylene molecules, the kinetics for *p*-xylene obeyed standard Michaelis–Menten kinetics. However, *m*-xylene is a better substrate for CYP2A6 than *p*-xylene (Tables 2 and 3), and the analytical sensitivity for *m*-xylene products was superior compared to the sensitivity for *p*-xylene products. Therefore, kinetic experiments with *m*-xylene could be conducted at the lower substrate concentrations where cooperative kinetics are most likely to be observed. We speculate that CYP2A6 can also accommodate multiple *p*-xylene ligands and that atypical kinetics may be observed at lower substrate concentrations because incubations containing both *m*- and *p*-xylene lead to heterotropic allosteric effects (Table 6).

The heterotropic experiments with *m*- and *p*-xylene provide significant new information (Table 6). Incubations at lower concentrations (60 μM; near the K_M) of *p*-xylene do not reveal changes to the *m*-xylene-α-$^2H_3$ product ratio (*m*-methylbenzylalcohol:2,4-dimethylphenol). However, at higher *p*-xylene concentrations (200 μM; above the K_M), a large decrease in product ratio (6.8 compared to 2.4) is observed. The product ratio at 200 μM *p*-xylene was even lower than that observed with 1 mM *m*-xylene-α-$^2H_3$ (2.4 ± 0.2 and 4.8 ± 0.3, respectively). Therefore, clearly CYP2A6 accommodates *p*-xylene and *m*-xylene simultaneously, and apparently, the heterotropic effects of *p*-xylene restrict *m*-xylene motion more than *m*-xylene homotropic effects, since aromatic hydroxylation becomes even more favored than with *m*-xylene alone. The same experiments with d_6-labeled *p*-xylene provide further insight.

Incubations with labeled *p*-xylene at 60 μM with 15 μM *m*-xylene-α-$^2H_3$ (both concentrations below the K_M and S_{50}, respectively) resulted in a change in the *m*-xylene product ratio that was observed only at a higher concentration (200 μM) of unlabeled *p*-xylene (product ratios of 3.3 and 6.8 at 60 μM labeled and unlabeled *p*-xylene, respectively). In terms of isotope effects, at 60 μM *p*-xylene there is an inverse isotope effect on 2,4-dimethylphenol formation [$(k_H/k_D)_{obs}$ = 0.49]. That is, 2,4-dimethylphenol formation, which is generated from *m*-xylene, is more favored in the presence of labeled *p*-xylene versus unlabeled *p*-xylene; deuterium labeling of the *p*-isomer leads to an isotope effect on the products formed by the *m*-isomer. This result unambiguously demonstrates simultaneous occupancy of *m*-xylene and *p*-xylene within a single active site. It is directly analogous to the observations of Jones et al. (*15*).

There are several sites for oxidation when *p*-xylene and *m*-xylene occupy the active site simultaneously under nonsaturating conditions. The most reactive sites are the benzylic positions of *p*-xylene or the unlabeled methyl group of *m*-xylene-α-$^2H_3$. There also are oxidation sites that are relatively less favored: aromatic hydroxylation on either *p*-xylene or *m*-xylene, or benzylic hydroxylation at the deuterium-labeled methyl group in *m*-xylene. If these substrates are interacting in the active site dynamically and rapidly (compared to the rate of the oxidizing step), then when the active-oxygenating species is presented with the deuterium-labeled methyl group of *m*-xylene it may instead "switch to" oxidation on the aromatic ring of *m*-xylene or benzylic oxidation of *p*-xylene. However, if *p*-xylene is deuterium-labeled, then it is no longer one of the relatively favorable sites of oxidation. Thus, there are fewer favorable options presented to the active oxygenating species, and therefore, aromatic hydroxylation of *m*-xylene occurs at a faster rate. The same effect was observed when the concentration of unlabeled *p*-xylene was increased, conceivably due to steric crowding. At concentrations approaching saturation for *p*-xylene and at low concentrations of *m*-xylene, those CYP2A6 molecules with *m*-xylene in the active site also have *p*-xylene present, and this apparently decreases the dynamics of *m*-xylene in the active site such that the rate of aromatic hydroxylation increases.

The results require an additional comment regarding Table 6. One of the original hypotheses tested here was that the measured intramolecular isotope effect, $(k_H/k_D)_{obs}$, should change in cases where a CYP binds multiple substrates in an active site (for the symmetrical substrates under study). A change is expected because multiple-ligand binding should lead to changes in steric constraints that affect rates of substrate reorientation, which is an important factor in intrinsic isotope effect suppression. In the results discussed thus far, dramatic suppression of $(k_H/k_D)_{obs}$ was not observed. Rather, the decrease in substrate dynamics was expressed as an increase in metabolic switching while $(k_H/k_D)_{obs}$ remained relatively constant. In other cases, it is possible that $(k_H/k_D)_{obs}$ values are generated from multiple substrates in the active site, and these substrates still have relatively high mobility in the active site. For example, two *p*-xylene molecules that are π-stacked could take up less active site volume than a single dimethylnaphthalene molecule (*p*-xylene volume, 103 Å^3; dimethylnaphthalene volume, 271 Å^3). Perhaps this is why the $(k_H/k_D)_{obs}$ values for these two substrates are not profoundly different (*39*). To test this hypothesis further with these substrate−P450 combinations, experiments will require higher enzyme concentrations and very low substrate concentrations so that products from incubations containing very small quantities of substrate can be measured accurately. In this study, with *m*-xylene, we were perhaps approaching this situation, but instead of seeing an elevation of the $(k_H/k_D)_{obs}$ at low substrate concentrations, we observed a decrease in branching (as discussed above, an increase in branching leads to elevation of the observed

isotope effect). The $(k_H/k_D)_{obs}$ values in Table 6 provide some evidence that steric crowding and decreased second substrate dynamics can be observed from a suppression of the measured isotope effect in addition to changes in metabolic switching.

In Table 6, the $(k_H/k_D)_{obs}$ for the sample that contained 200 μM d_6-*p*-xylene is statistically different and suppressed compared to those values under all the other experimental conditions (e.g., 5.77 $\pm$ 0.45 versus 7.22 $\pm$ 0.48 observed for unlabeled *p*-xylene and 6.98 $\pm$ 0.16 for 15 μM *m*-xylene-α-$^2H_3$ alone). More experimentation is required as the difference, albeit statistically significant, is not profound. Theoretically, it is plausible that the $(k_H/k_D)_{obs}$ is suppressed with d_6-*p*-xylene, because this effector molecule is less reactive, with regard to P450-mediated oxidation, than the other unlabeled effectors (e.g., a second *m*-xylene molecule or unlabeled *p*-xylene). So, if the effector molecule is itself readily oxidized by P450, then k_H/k_D suppression is less likely to be observed because the effector substrate (heterotropic or homotropic) provides another branching route.

In conclusion, this work has provided several lines of evidence that CYP2A6 accommodates multiple ligands and this can lead to homotropic and heterotropic effects. One piece of evidence is that CYP2A6-mediated *m*-xylene-α-$^2H_3$ oxidation exhibits nonlinear Eadie−Hofstee plots. Also, this enzyme–substrate pair displays a concentration-dependent decrease in product ratio for *m*-xylene-α-$^2H_3$ oxidation, and this ratio is further reduced by the presence of 200 μM *p*-xylene or 60 μM d_6-labeled *p*-xylene. Furthermore, an inverse deuterium isotope effect on 2,4-dimethylphenol formation generated via the labeling of a heterotropic effector (*p*-xylene) points to a molecular mechanism that involves two substrates bound simultaneously to the CYP2A6 active site. Thus, the overall evidence indicates that intramolecular isotope effect experiments can be used to provide insight into the molecular mechanisms of P450 allosterism by exhibiting how an effector molecule can affect the dynamics of a substrate in the active site. That is, a significant increase in isotopically sensitive branching did not lead to an increase in the $(k_H/k_D)_{obs}$ for *m*-xylene-α-$^2H_3$ oxidation, suggesting that there must be a decrease in the rate of reorientation of *m*-xylene-α-$^2H_3$. Also, there is a suppression of the $(k_H/k_D)_{obs}$ for *m*-xylene-α-$^2H_3$ oxidation with increasing concentrations of deuterium-labeled *p*-xylene. It should be possible to further refine conditions (perhaps by using hexafluoro-*p*-xylene) so that changes in the measured $(k_H/k_D)_{obs}$ can provide explicit changes in the substrate dynamics induced by effector molecules.

ACKNOWLEDGMENT

We thank Kent Kunze and Josh Pearson for thoughtful discussion.

SUPPORTING INFORMATION AVAILABLE

A table of product formation rates and corresponding product ratios as a function of substrate concentration for the CYP2A6-mediated oxidation of *m*-xylene-α-$^2H_3$, a typical standard curve used to quantify *m*-methylbenzylalcohol and 2,4-dimethylphenol, and tables of peak areas utilized to generate Table 6 and Figures 5 and 6. This material is available free of charge via the Internet at http://pubs.acs.org.

REFERENCES

1. Ortiz de Montellano, P. R. (2004) *Cytochrome P450: Structure, Mechanism, and Biochemistry*, 3rd ed., Springer-Verlag LLC, New York.
2. Schenkman, J. B., and Jansson, I. (2003) The many roles of cytochrome b5. *Pharmacol. Ther. 97*, 139–152.
3. Atkins, W. M. (2005) Non-Michaelis-Menten kinetics in cytochrome P450-catalyzed reactions. *Annu. Rev. Pharmacol. Toxicol. 45*, 291–310.
4. Schrag, M. L., and Wienkers, L. C. (2000) Topological alteration of the CYP3A4 active site by the divalent cation Mg^{2+}. *Drug Metab. Dispos. 28*, 1198–1201.
5. Lasker, J. M., Huang, M. T., and Conney, A. H. (1982) In vivo activation of zoxazolamine metabolism by flavone. *Science 216*, 1419–1421.
6. Hutzler, J. M., Powers, F. J., Wynalda, M. A., and Wienkers, L. C. (2003) Effect of carbonate anion on cytochrome P450 2D6-mediated metabolism in vitro: The potential role of multiple oxygenating species. *Arch. Biochem. Biophys. 417*, 165–175.
7. Atkins, W. M. (2006) Current views on the fundamental mechanisms of cytochrome P450 allosterism. *Expert Opin. Drug Metab. Toxicol. 2*, 573–579.
8. Maenpaa, J., Hall, S. D., Ring, B. J., Strom, S. C., and Wrighton, S. A. (1998) Human cytochrome P450 3A (CYP3A) mediated midazolam metabolism: The effect of assay conditions and regioselective stimulation by α-naphthoflavone, terfenadine and testosterone. *Pharmacogenetics 8*, 137–155.
9. Guengerich, F. P. (1999) Cytochrome P-450 3A4: Regulation and role in drug metabolism. *Annu. Rev. Pharmacol. Toxicol. 39*, 1–17.
10. Schoch, G. A., Yano, J. K., Wester, M. R., Griffin, K. J., Stout, C. D., and Johnson, E. F. (2004) Structure of human microsomal cytochrome P450 2C8. Evidence for a peripheral fatty acid binding site. *J. Biol. Chem. 279*, 9497–9503.
11. Williams, P. A., Cosme, J., Vinkovic, D. M., Ward, A., Angove, H. C., Day, P. J., Vonrhein, C., Tickle, I. J., and Jhoti, H. (2004) Crystal structures of human cytochrome P450 3A4 bound to metyrapone and progesterone. *Science 305*, 683–686.
12. Yano, J. K., Wester, M. R., Schoch, G. A., Griffin, K. J., Stout, C. D., and Johnson, E. F. (2004) The structure of human microsomal cytochrome P450 3A4 determined by X-ray crystallography to 2.05-Å resolution. *J. Biol. Chem. 279*, 38091–38094.
13. Korzekwa, K. R., Krishnamachary, N., Shou, M., Ogai, A., Parise, R. A., Rettie, A. E., Gonzalez, F. J., and Tracy, T. S. (1998) Evaluation of atypical cytochrome P450 kinetics with two-substrate models: Evidence that multiple substrates can simultaneously bind to cytochrome P450 active sites. *Biochemistry 37*, 4137–4147.
14. Cupp-Vickery, J., Anderson, R., and Hatziris, Z. (2000) Crystal structures of ligand complexes of P450eryF exhibiting homotropic cooperativity. *Proc. Natl. Acad. Sci. U.S.A. 97*, 3050–3055.
15. Rock, D. A., Perkins, B. N., Wahlstrom, J., and Jones, J. P. (2003) A method for determining two substrates binding in the same active site of cytochrome P450BM3: An explanation of high energy omega product formation. *Arch. Biochem. Biophys. 416*, 9–16.
16. Lampe, J. N., and Atkins, W. M. (2006) Time-resolved fluorescence studies of heterotropic ligand binding to cytochrome P450 3A4. *Biochemistry 45*, 12204–12215.
17. Dabrowski, M. J., Schrag, M. L., Wienkers, L. C., and Atkins, W. M. (2002) Pyrene·pyrene complexes at the active site of cytochrome P450 3A4: Evidence for a multiple substrate binding site. *J. Am. Chem. Soc. 124*, 11866–11867.
18. Vaz, A. D., Pernecky, S. J., Raner, G. M., and Coon, M. J. (1996) Peroxo-iron and oxenoid-iron species as alternative oxygenating agents in cytochrome P450-catalyzed reactions: Switching by threonine-302 to alanine mutagenesis of cytochrome P450 2B4. *Proc. Natl. Acad. Sci. U.S.A. 93*, 4644–4648.
19. Wen, B., Lampe, J. N., Roberts, A. G., Atkins, W. M., David Rodrigues, A., and Nelson, S. D. (2006) Cysteine 98 in CYP3A4 contributes to conformational integrity required for P450 interaction with CYP reductase. *Arch. Biochem. Biophys. 454*, 42–54.
20. Spatzenegger, M., Liu, H., Wang, Q., Debarber, A., Koop, D. R., and Halpert, J. R. (2003) Analysis of differential substrate selectivities of CYP2B6 and CYP2E1 by site-directed mutagenesis and molecular modeling. *J. Pharmacol. Exp. Ther. 304*, 477–487.
21. Khan, K. K., He, Y. Q., Domanski, T. L., and Halpert, J. R. (2002) Midazolam oxidation by cytochrome P450 3A4 and active-site mutants: An evaluation of multiple binding sites and of the

metabolic pathway that leads to enzyme inactivation. *Mol. Pharmacol. 61*, 495–506.
22. Domanski, T. L., He, Y. A., Harlow, G. R., and Halpert, J. R. (2000) Dual role of human cytochrome P450 3A4 residue Phe-304 in substrate specificity and cooperativity. *J. Pharmacol. Exp. Ther. 293*, 585–591.
23. Williams, P. A., Cosme, J., Ward, A., Angove, H. C., Matak Vinkovic, D., and Jhoti, H. (2003) Crystal structure of human cytochrome P450 2C9 with bound warfarin. *Nature 424*, 464–468.
24. Scott, E. E., He, Y. A., Wester, M. R., White, M. A., Chin, C. C., Halpert, J. R., Johnson, E. F., and Stout, C. D. (2003) An open conformation of mammalian cytochrome P450 2B4 at 1.6-Å resolution. *Proc. Natl. Acad. Sci. U.S.A. 100*, 13196–13201.
25. Scott, E. E., White, M. A., He, Y. A., Johnson, E. F., Stout, C. D., and Halpert, J. R. (2004) Structure of mammalian cytochrome P450 2B4 complexed with 4-(4-chlorophenyl)imidazole at 1.9-Å resolution: Insight into the range of P450 conformations and the coordination of redox partner binding. *J. Biol. Chem. 279*, 27294–27301.
26. Smith, S. V., Koley, A. P., Dai, R., Robinson, R. C., Leong, H., Markowitz, A., and Friedman, F. K. (2000) Conformational modulation of human cytochrome P450 2E1 by ethanol and other substrates: A CO flash photolysis study. *Biochemistry 39*, 5731–5737.
27. Prasad, S., Mazumdar, S., and Mitra, S. (2000) Binding of camphor to *Pseudomonas putida* cytochrome $p450_{cam}$: Steady-state and picosecond time-resolved fluorescence studies. *FEBS Lett. 477*, 157–160.
28. Prasad, S., and Mitra, S. (2002) Role of protein and substrate dynamics in catalysis by *Pseudomonas putida* cytochrome P450cam. *Biochemistry 41*, 14499–14508.
29. Davydov, D. R., Botchkareva, A. E., Kumar, S., He, Y. Q., and Halpert, J. R. (2004) An electrostatically driven conformational transition is involved in the mechanisms of substrate binding and cooperativity in cytochrome P450eryF. *Biochemistry 43*, 6475–6485.
30. Jovanovic, T., and McDermott, A. E. (2005) Observation of ligand binding to cytochrome P450 BM-3 by means of solid-state NMR spectroscopy. *J. Am. Chem. Soc. 127*, 13816–13821.
31. Lee, H., Ortiz de Montellano, P. R., and McDermott, A. E. (1999) Deuterium magic angle spinning studies of substrates bound to cytochrome P450. *Biochemistry 38*, 10808–10813.
32. Gillette, J. R., Darbyshire, J. F., and Sugiyama, K. (1994) Theory for the observed isotope effects on the formation of multiple products by different kinetic mechanisms of cytochrome P450 enzymes. *Biochemistry 33*, 2927–2937.
33. Darbyshire, J. F., Gillette, J. R., Nagata, K., and Sugiyama, K. (1994) Deuterium isotope effects on A-ring and D-ring metabolism of testosterone by CYP2C11: Evidence for dissociation of activated enzyme-substrate complexes. *Biochemistry 33*, 2938–2944.
34. Regal, K. A., Kunze, K. L., Peter, R. M., and Nelson, S. D. (2005) Oxidation of caffeine by CYP1A2: Isotope effects and metabolic switching. *Drug Metab. Dispos. 33*, 1837–1844.
35. Nelson, S. D., and Trager, W. F. (2003) The use of deuterium isotope effects to probe the active site properties, mechanism of cytochrome P450-catalyzed reactions, and mechanisms of metabolically dependent toxicity. *Drug Metab. Dispos. 31*, 1481–1498.
36. Iyer, K. R., Jones, J. P., Darbyshire, J. F., and Trager, W. F. (1997) Intramolecular isotope effects for benzylic hydroxylation of isomeric xylenes and 4,4′-dimethylbiphenyl by cytochrome P450: Relationship between distance of methyl groups and masking of the intrinsic isotope effect. *Biochemistry 36*, 7136–7143.
37. Henne, K. R., Fisher, M. B., Iyer, K. R., Lang, D. H., Trager, W. F., and Rettie, A. E. (2001) Active site characteristics of CYP4B1 probed with aromatic ligands. *Biochemistry 40*, 8597–8605.
38. Rock, D. A., Boitano, A. E., Wahlstrom, J. L., Rock, D. A., and Jones, J. P. (2002) Use of kinetic isotope effects to delineate the role of phenylalanine 87 in P450(BM-3). *Bioorg. Chem. 30*, 107–118.
39. Harrelson, J. P., Henne, K. R., Alonso, D. O., and Nelson, S. D. (2007) A comparison of substrate dynamics in human CYP2E1 and CYP2A6. *Biochem. Biophys. Res. Commun. 352*, 843–849.
40. Tracy, T. S., Hutzler, J. M., Haining, R. L., Rettie, A. E., Hummel, M. A., and Dickmann, L. J. (2002) Polymorphic variants (CYP2C9*3 and CYP2C9*5) and the F114L active site mutation of CYP2C9: Effect on atypical kinetic metabolism profiles. *Drug Metab. Dispos. 30*, 385–390.
41. Kenworthy, K. E., Clarke, S. E., Andrews, J., and Houston, J. B. (2001) Multisite kinetic models for CYP3A4: Simultaneous activation and inhibition of diazepam and testosterone metabolism. *Drug Metab. Dispos. 29*, 1644–1651.
42. Korzekwa, K. R., Trager, W. F., and Gillette, J. R. (1989) Theory for the observed isotope effects from enzymatic systems that form multiple products via branched reaction pathways: Cytochrome P-450. *Biochemistry 28*, 9012–9018.
43. Harada, N., Miwa, G. T., Walsh, J. S., and Lu, A. Y. (1984) Kinetic isotope effects on cytochrome P-450-catalyzed oxidation reactions. Evidence for the irreversible formation of an activated oxygen intermediate of cytochrome P-448. *J. Biol. Chem. 259*, 3005–3010.
44. Jones, J. P., Korzekwa, K. R., Rettie, A. E., and Trager, W. F. (1986) Isotopically Sensitive Branching and Its Effect on the Observed Intramolecular Isotope Effects in Cytochrome P-450 Catalyzed Reactions: A New Method for the Estimation of Intrinsic Isotope Effects. *J. Am. Chem. Soc. 108*, 7074–7078.
45. Roberts, A. G., Campbell, A. P., and Atkins, W. M. (2005) The thermodynamic landscape of testosterone binding to cytochrome P450 3A4: Ligand binding and spin state equilibria. *Biochemistry 44*, 1353–1366.
46. Lin, Y., Lu, P., Tang, C., Mei, Q., Sandig, G., Rodrigues, A. D., Rushmore, T. H., and Shou, M. (2001) Substrate inhibition kinetics for cytochrome P450-catalyzed reactions. *Drug Metab. Dispos. 29*, 368–374.
47. Yano, J. K., Hsu, M. H., Griffin, K. J., Stout, C. D., and Johnson, E. F. (2005) Structures of human microsomal cytochrome P450 2A6 complexed with coumarin and methoxsalen. *Nat. Struct. Mol. Biol. 12*, 822–823.
48. Venkatakrishnan, K., von Moltke, L. L., and Greenblatt, D. J. (1998) Human cytochromes P450 mediating phenacetin O-deethylation in vitro: Validation of the high affinity component as an index of CYP1A2 activity. *J. Pharm. Sci. 87*, 1502–1507.

BI702020Y